Scholarly Research Journal for Interdisciplinary Studies,
Online ISSN 2278-8808, SJIF 2021 = 7.380, www.srjis.com
PEER REVIEWED & REFEREED JOURNAL, MAR-APRIL, 2021, VOL- 8/64

ELECTRONIC STRUCTURE AND MAGNETIC AND OPTICAL PROPERTIES OF TRANSITION-METAL DINUCLEAR MOLECULES: A THEORETICAL INVESTIGATION

Surendra Singh, Ph. D.

M.Sc., M.Phil., Ph.D., Associate Professor, Dept of Chemistry, Govt. Degree College, Mant, Mathura (U.P.)

Paper Received On: 21 APRIL 2021
Peer Reviewed On: 30 APRIL 2021
Published On: 1 MAY 2021

Abstract

In the present work, we've reported the electronic structure, spin state, and optical properties of a replacement class of transition-metal (TM) dinuclear molecules (TM = Cr, Mn, Fe, Co, and Ni). the steadiness of those molecules has been analyzed from the vibration spectra obtained by using density functional theory (DFT) calculations. The ground-state spin configuration of the tetra-coordinated TM atom in each molecule has been predicted from the relative total energy differences in several spin states of the molecule. The DFT + U method has been accustomed investigate the precise ground-state spin configuration of every molecule. We further performed time-dependent DFT calculations to check the optical properties of those molecules. The planar geometric structure remains intact in most of the cases; hence, these molecules are expected to be adsorbed and self-assembled on metal substrates. additionally, the optical characterization of those molecules indicates that the absorption spectra have an outsized peak within the blue-light wavelength range; therefore, it can be suitable for advanced optoelectronic device applications. Our work promotes further computational and experimental studies on TM dinuclear molecules within the field of molecular spintronics and optoelectronics.

***Keywords**: Electronic Structure, Optical Properties, Transition-Metal, Dinuclear Molecules, Investigation*

Introduction

Quinonoids are promising molecules, well-known for his or her application in several chemical and organic process.1,2 This class of molecules and their derivatives are highly pH-selective and pH-sensitive.3−5 Their presence in organic thin films may significantly enhance the charge carrier concentration of films. As a result highly conductive interface will be

formed by adsorbing these molecules and their derivatives on metal/semiconducting surfaces.6 These ascribe that considering quinonoids and their derivatives as active centers, one can participate in developing new functional materials. additionally, metal–organic quinonoid molecules are potential building blocks in coordination polymers furthermore as many other materials which are useful for catalysis, surface chemistry, and molecular spintronics.7,8

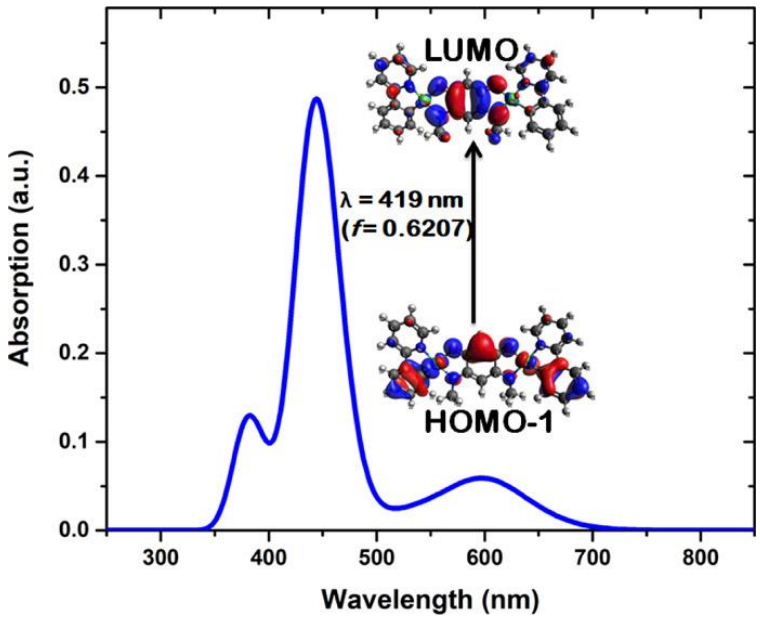

In transition-metal-quinonoid (TM-quinonoid), the valence electrons are primarily from the partially filled d-orbitals of the TM. Therefore, they'll be stabilize in various spin-state configurations betting on the local environment of the TM present within the molecule. As a result, this class of materials could exhibit reversible spin state switching under the influence of suitable external parameters like temperature, pressure, electric, and field of force. Molecules which exhibit reversible spin switching are useful for memory storage devices and molecular switches. Mixed valence and valence tautomerism in TM-quinonoid complexes have already been reported and may be exploited in molecular switching applications.8 Recently, a multifunctional Ni-quinonoid molecule has been reported during which a Ni atom connects two quinonoid molecules, exhibits a reversible color change, and undergoes structural transformation upon methanol adsorption.9 In one amongst our previous report, we've got shown that the Ni-quinonoid molecule chemisorbed on the Co(100) surface, coupled ferromagnetically with the substrate, during which the Ni spin state switches from

low spin (LS) to high spin (HS).10 Several quinonoid-based organometallic compounds are synthesized within the past few years, planning to their application in spintronics. Kar et al.11 have recently reported quinonoid-based homo- and hetero-dinuclear complexes, where the 2 noble metals (PtII and/or PdII) are linked through a quinonoid molecule. they need also reported that the metal center will be replaced with TM by using suitable precursor during the synthesis process. Herein, we modeled a group of TM homo-dinuclear organometallics like the reported PtII-dinuclear complex, by replacing both the noble metals within the molecule with different TM atoms and allotted theoretical investigations of their stability, electronic structure, magnetic, and optical properties by using density functional theory (DFT) calculations.

Computational Methodology

TM dinuclear molecules were modeled in line with the reported structure of the PtII-dinuclear complex.11 Electronic structure and optical absorption spectra of those molecules were obtained by using DFT calculations implemented within the GAUSSIAN 09 package.12 The all-electron Gaussian basis set developed by Ahlrichs and co-workers13 was employed for all the weather in each system. Prediction of proper ground-state spin configuration of organometallic molecules could be a challenging task because the total energy difference can be very small for such complex in several spin-state configuration.14 Recent studies showed that the meta-GGA hybrid functional (TPSSh functional)15,16 which uses 10% Hartree–Fock exchange to approximate the exchange correlation functional for TM atoms works excellently and predicts accurate spin configurations in TM-organometallic complexes.17 Hence, we've used the TPSSh functional with the big triple-ζ basis set13 together with polarization function for all the atoms. The geometric structure of all the molecules were optimized using this functional. Bernys optimization algorithm which involves redundant internal coordinates was wont to optimize the molecular geometry.

The detailed magnetic structure of TM-organometallics was obtained by using the plane wave, pseudopotential method as implemented within the Vienna initially Simulation Package (VASP)18 with projected augmented plane wave potential.19 Generalized gradient approximation (GGA) was used with Perdew–Burke–Ernzerhof parameterization for exchange–correlation function.20 we've used DFT + U technique21 to get the precise spin state of the organometallic by capturing the strong electron–electron correlation effect within

the partially filled 3d shell of TM atoms and missing correlation effect beyond GGA. we've got tested with different on-site Coulomb parameter (U) and exchange parameter (J) for TM atoms. This method has already been proven to be very accurate in similar systems.22−25 an in depth description is given in Supporting Information. A plane wave mechanical energy cutoff of 500 eV was considered. The convergence criterion was set to 10–5 eV for the self-consistent electronic minimization. Forces on each atom were estimated using the Hellmann–Feynman theorem, and subsequently, structural optimization was allotted using the conjugate gradient method until force on each atom was reduced to 0.01 eV/Å.

Results and Discussion

Optimized Geometric Structure

The molecular structure of the TM dinuclear molecule incorporates two TM atoms, one quinonoid and two bipyridine ligands. Every one of two TM atoms within the molecule is attached with a bipyridine ligand. TM atoms are further connected through a quinonoid. The modeled structure of the TM dinuclear molecule is shown in Figure Figure11a. so as to proceed further, we first optimized the geometric structure and investigated the vibrational spectra of every modeled molecule to check their structural stability.26,27 The calculated IR spectra of TM dinuclear molecules is given in Figure S1. The absence of any negative frequencies in vibration spectra confirms that the optimized structures of molecules are stable. Although the fundamental structures of of these molecules are same, there are conformal changes, clearly visible within the molecule with different TM atoms. The typical TM–ligand bond lengths (ΔTM – L) are 2.05, 2.09, 1.95, 1.93, and 1.90 Å for Cr, Mn, Fe, Co, and Ni dinuclear molecules, respectively. We observed distortion of the molecular planer structure round the TM atom site, which is different in numerous molecules looking on the TM atom. The distortion from a square-planar to a tetrahedral structure may be indexed with the τ4 parameter; τ4 is 0 for the proper square-planar and 1 for the proper tetrahedral geometry. The τ4 parameter within the tetra-coordinated geometry of molecules was calculated from the relation $\tau4 = (360° - (\theta + \Phi))/141°$, where θ (O–TM–C) and Φ [N(1)–TM–N(2)] are the 2 largest angles within the tetra-coordinated geometry. The τ4 parameter for the distortion within the tetra-coordinated TM of the molecules is tabulated in Table 1.

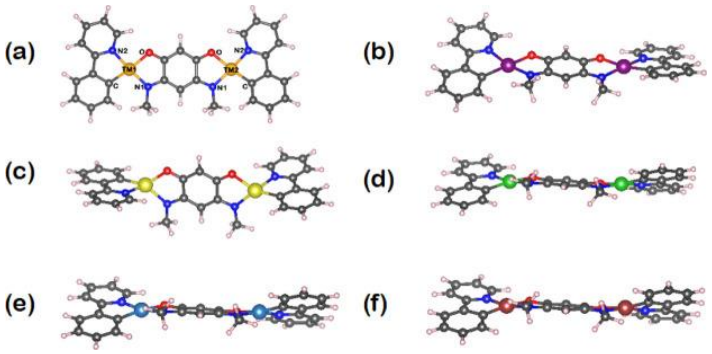

Figure 1: (a) Modelled structure of the TM dinuclear molecule; TM, O, N, C, and H atoms are represented by orange, red, blue, black, and light pink colored balls, respectively. (b–f) Optimized structure of the Cr^{II}-, Mn^{II}-, Fe^{II}-, Co^{II}-, and Ni^{II}-dinuclear molecules. Cr, Mn, Fe, Co, and Ni atoms are represented by magenta, yellow, turquoise, and bronze, respectively, whereas other atoms are shown same as in (a).

Table 1-Calculated Average TM–Ligand Bond Lengths (in Å) and the Distortion Parameter in the Optimized Geometry of TM Dinuclear Molecules

		average TM–ligand bond length in (Å)		**τ_4**	
molecule	**TM**	**TPSSh**	**GGA + *U***	**TPSSh**	**GGA + *U***
Cr^{II}	Cr-1	2.05847	2.07833	0.16	0.16
	Cr-2	2.05846	2.07840	0.16	0.16
Mn^{II}	Mn-1	2.09841	2.14652	0.75	0.38
	Mn-2	2.09840	2.14627	0.75	0.38
Fe^{II}	Fe-1	1.95588	1.96381	0.15	0.16
	Fe-2	1.95589	1.96376	0.15	0.16
Co^{II}	Co-1	1.93057	1.92874	0.17	0.17
	Co-2	1.93058	1.92900	0.17	0.17
Ni^{II}	Ni-1	1.90151	1.90319	0.16	0.16
	Ni-2	1.90148	1.90323	0.16	0.16

Our investigation shows that the tetra-coordinated Mn atoms in MnII-dinuclear molecule is more distorted toward tetrahedral geometry compared to other TM dinuclear molecules, which are nearly within the square-planar geometry. in line with the well-known Irving–Williams order,28 the soundness of the TM increases within the order MnII < FeII < CoII < NiII. Therefore, the distortion within the MnII-dinuclear molecule may well be ascribed due to less ligand field stabilization energy.29 Optimized geometry for every of those molecules is shown in Figure Figure11b–f.

Electronic Structure and Magnetic Properties

The magnetic behavior of TM dinuclear molecules depends on the coordination of TM and their local environment. In general, tetra-coordinated (square-planar) TM centers with over half-filled d-orbitals don't exhibit the HS state thanks to an oversized John–Tellar effect.9 Therefore, reckoning on the amount of electrons present in d-orbitals of the TM atom, the spin state of the magnetic center of those organometallic molecules are expected to be either intermediate spin (IS) or LS state. Hence one amongst singlet, triplet, and quintuplet would be the possible spin states (or spin multiplicities) for the molecule with a fair number of electrons within the d-orbitals, whereas the doublet, quartet, or sextet would be the possible spin states for those with an odd number of electrons within the d-orbitals. The ground-state spin configuration of the organometallic molecules made up our minds by comparing the full energies of the molecule calculated all told the possible spin-state configurations. The difference in total energy with relevance the ground-state energy in several spin states is listed in Table 2. Our calculations show that the CrII- and MnII-dinuclear molecules are in HS state configuration, FeII-dinuclear is in IS state configuration, and CoII- and NiII-dinuclear molecules are in LS state configuration in their respective state. The obtained average TM-ligand bond lengths (ΔTM – L) of the optimized structures for the LS and HS states are within the range of 1.90–1.93 and 2.07–2.15 Å, respectively, and ≈1.96 Å for the IS state, and these values are in good agreement with the reported ΔTM – L values for the respective spin state of the organometallic molecules.22,30 Note that the energy change thanks to the change of the spin state within the TM atom within the molecule is significantly high; this is often mainly due to the local environment of the TM atom within the optimized structure of the molecule, which strongly affects on the occupation of d-orbitals.

Table 2-Calculated Total Energy Difference in the Possible Spin States with Respect to the Ground Spin-State Energy of the TM-Dinuclear Molecules in eV[a]

	relative total energy and spin state (in eV)		
molecule	**LS**	**IS**	**HS**
Cr^{II}	5.08 (singlet)	1.263 (triplet)	0 (quintuplet)
Mn^{II}	2.19 (doublet)	0.296 (quartet)	0 (sextet)
Fe^{II}	2.22 (singlet)	0 (triplet)	0.92 (quintuplet)
Co^{II}	0 (doublet)		0.63 (quartet)
Ni^{II}	0 (singlet)		1.86 (triplet)

[a]Total energy = 0 eV represents the ground-state spin configuration. Corresponding spin multiplicity of TM is given in parentheses.

In order to possess a transparent insight into the anticipated spin state, we further performed the GGA + U calculations and obtained detailed atom-specific spin moments of molecules. The obtained moment of a magnet on the both the TM atoms in each molecule is listed in Table 3.

Table 3-Calculated Magnetic Moments and Spin State (in Parenthesis) on the TM Atoms in TM Dinuclear Molecules

	magnetic Moment (in μ_B)		
molecule	**TM-1**	**TM-2**	**total magnetic moment of the molecule (in μ_B)**
Cr^{II}	3.730 (*S* = 2)	3.730 (*S* = 2)	8.0
Mn^{II}	4.598 (*S* = 5/2)	4.598 (*S* = 5/2)	10.0
Fe^{II}	2.149 (*S* = 1)	2.149 (*S* = 1)	4.0
Co^{II}	1.083 (*S* = 1/2)	1.083 (*S* = 1/2)	2.0
Ni^{II}	–0.012 (*S* = 0)	–0.012 (*S* = 0)	0.0

To understand the electron occupation within the d-orbitals, we've got obtained the spin and d-orbital resolved density of states (DOSs) for every molecule, as plotted in Figure Figure22a–e. TM atoms in molecules are tetra-coordinated and bonded with O, N, and C atoms of molecular ligands within the xy-plane. Therefore, σ-type hybridization between the in-plane 3d and 2p orbitals will originate the crystal field effect in d-orbitals of TM atoms. The coulomb repulsion together with strong σ-type hybridization will result in a splitting of the d-orbital into t2g and eg orbitals. On the opposite hand, within the absence of vertical co-ordination of TM, the degenerated eg orbitals will further split into two states, during which the dz2–r2 orbital are going to be lower in energy compared to $d_{x^2-y^2}$.

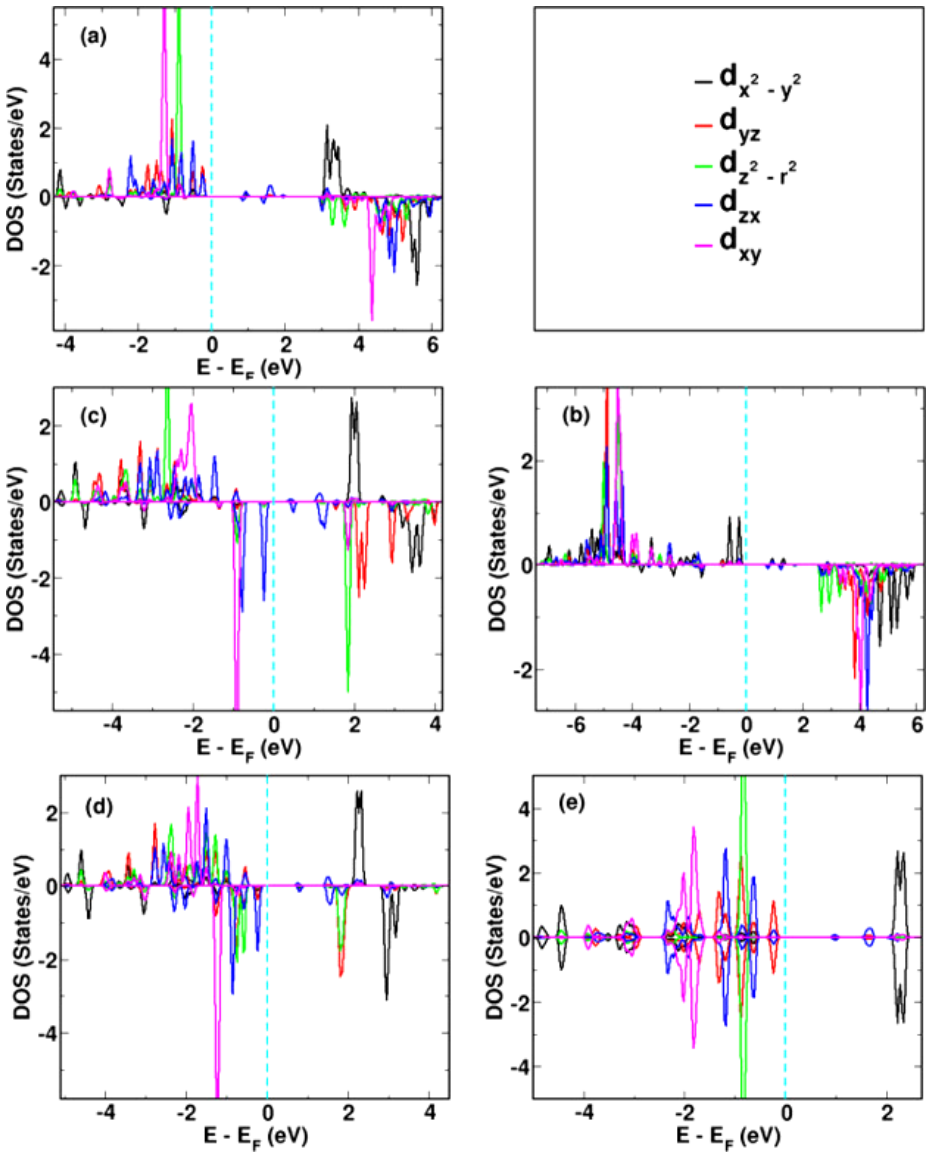

Figure 2: d-orbital projected DOS of the TM atom in (a) Cr^{II}-, (b) Mn^{II}-, (c) Fe^{II}-, (d) Co^{II}-, and (e) Ni^{II}-dinuclear molecule. Spin-up and spin-down DOS are shown by positive and negative values, respectively.

Relatively, shorter TM–ligand bond lengths in Fe-, Co-, and Ni-dinuclear will induce strong ligand field and affect the in-plane d-orbitals of the TM atom that may further raise the in-plane orbital energy levels. As a result, electron distribution within the d-orbital for 3d6–3d8 electronic configurations will violate the Hund's rule. Electrons are going to be forced to occupy the dxz, dyz, dz2–r2, and dxy orbitals first to saturate these orbitals, leaving the dx2–y2 orbital completely unoccupied. The d-orbital-projected DOSs for the system with 3d6–3d8 configurations are shown within the Figure Figure22a,c–e, which clearly shows that both the

up and down spin dx2–y2 states are within the conduction band. Within the case of the FeII-dinuclear complex, the dxz and dxy orbitals are completely occupied, and dyz and dz2–r2 orbitals are partially crammed with spin-up electrons. As a result, the spin state of the FeII atom clothed to be S = 1. During a similar way, only the dyz orbital in CoII-complex is partially full of spin-up electron and every one three dxz, dxy, dz2–r2 orbitals are completely occupied. Thus, the spin state of the CoII atom is S = 1/2 (see Figure Figure22d). within the case of NiII-dinuclear, all four dxz, dyz, dz2–r2, and dxy orbitals are completely occupied and therefore the dx2–y2 orbital is totally unoccupied, resulting in S = 0 spin state for this method, whereas within the case of the CrII-dinuclear molecule, these four orbitals are partially occupied with the spin-up electrons giving rise to S = 2 spin state during this system. Interestingly, MnII-dinuclear doesn't follow this rule. Because the tetra-coordinated Mn atoms in MnII-dinuclear molecule are more distorted towards tetrahedral geometry, also, the typical TM–ligand bond length is increased. Therefore, realignment of the d-orbitals per the tetrahedral co-ordination is anticipated. As a result, all the d-orbitals including the in-plane dx2–y2 orbital of Mn within the MnII-dinuclear molecule are singly occupied with spin-up electrons, and therefore the spin-down channel is totally empty. Hence, the spin state of the tetra-coordinated MnII atom within the molecule is clad to be S = 5/2.

Optical Properties

Optical response could be a great tool to grasp the correct electronic behavior of molecules. Therefore, considering the optimized structure of TM dinuclear molecules, we've performed time-dependent density functional theory (TD-DFT) calculations by using the PBE0 functional.31 The reconstructed LANL2DZ basis set has been considered for TM atoms, which are known to produce accurate excitation and ionization energies.32,33 we've calculated electronic transitions and absorption spectra within the UV–visible range. The optical absorption spectra of various TM dinuclear molecules are plotted in Figure Figure33. We observed that there are two major peaks within the absorption spectra. the primary one is within the range of 410–450 nm which has maximum intensity and therefore the second is within the range of 560–590 nm which is a smaller amount intense and wide. The position of the utmost intensity peaks, band transition energy, and transition probabilities of TM dinuclear molecules are listed within the Table 4. Maximum intensity of the primary peak is observed from the Ni-dinuclear molecule. An analogous but slightly less intensity peak is

found for the Co-dinuclear molecule. For other three TM dinuclear molecules, the optical phenomenon is kind of broad. Within the case of the Fe-dinuclear molecule, the primary and second peaks appear near 545 and 680 nm wavelength regions, respectively. From the optical absorption spectra, we are able to predict that the dinuclear molecule containing Cr, Ni, Co, and Mn atoms would be useful for blue semiconductor diode applications, during which the Ni-dinuclear molecule will show maximum efficiency. However, the Fe-dinuclear molecule would be useful for traffic signal emission.

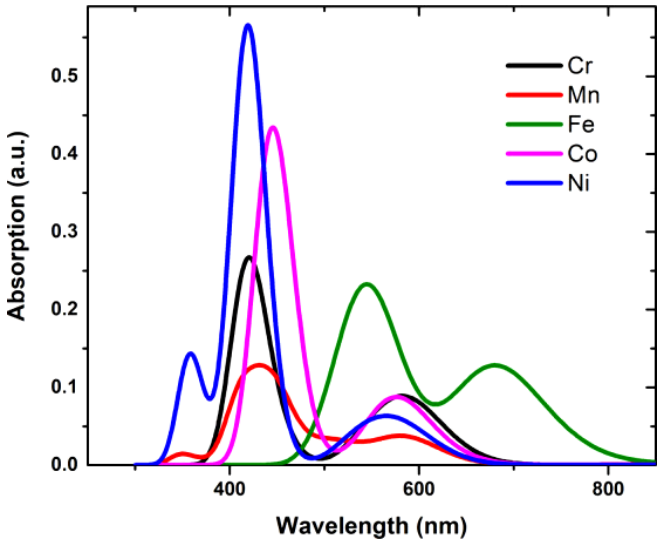

Figure 3: UV–vis absorption spectra of all TM dinuclear molecules obtained from TD-DFT calculations.

Table 4- Calculated Transition Energies, Absorption Wavelength, and Corresponding Transition Probabilities for TM-Dinuclear Molecules

molecule	transition energy (eV)	transition wavelength (λ) (nm)	transition probability
Cr^{II}	2.9807	415.95	0.0967
Mn^{II}	3.0063	412.42	0.1033
Fe^{II}	2.2483	551.45	0.2076
Co^{II}	2.7883	444.67	0.4664
Ni^{II}	2.9584	419.09	0.6207

To understand the nature of inter-/intraband transitions under the influence of photon absorption, we plotted the frontier orbitals for each system. Molecular orbital plots clearly

indicate that π-electrons in quinonoid (Q^{2-}) adopt a zwitterionic form with two delocalized subunits, that is, trimethine oxonol (OCCCO) and trimethine cyanine (NCCCN) in each molecule. Higher occupied orbitals especially the highest occupied molecular orbital (HOMO) and HOMO – 1 are mainly contributed either from NCCCN or OCCCO subunit orbitals in most of the cases. On the other hand, lower unoccupied orbitals are localized mainly on the electron deficient C–C single bond of the quinonoid ligand. Excitation wavelengths and their corresponding oscillator strengths which originates the absorption bands for Ni- and Co-dinuclear molecule are marked with arrows in Figure 4a,b, respectively.

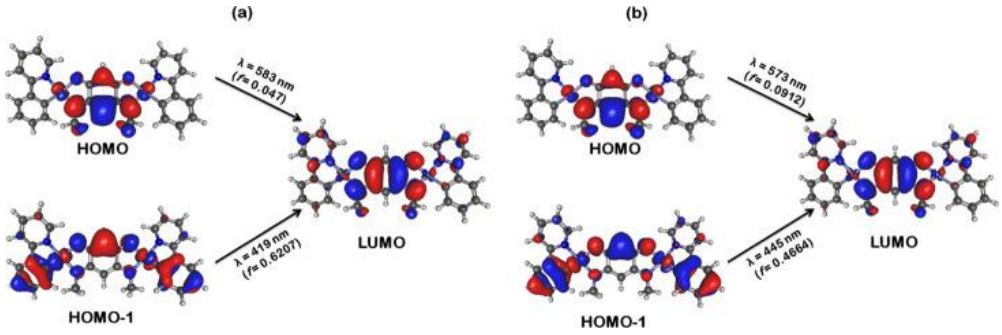

Figure 4: HOMO, HOMO – 1, and LUMO orbital plots for (a) Ni^{II}- and (b) Co^{II}-dinuclear molecule obtained from DFT calculations using the PBE0 functional. These are the main molecular orbital in which transition take places during the photo-absorption. Transition wavelength and corresponding transition probabilities are indicated near arrow marks.

The intense peaks within the absorption spectra of Ni-dinuclear and Co-dinuclear molecules are at λ = 420 nm and at λ = 446 nm, respectively, and are mainly attributed to the (HOMO – 1)–LUMO transition in both cases. However, the HOMO–LUMO transition in both cases corresponds to the broad optical phenomenon which are at λ = 566 nm and at λ = 577 nm for Ni- and Co-molecules, respectively.

Conclusions

To conclude, we've studied the electronic structure, magnetic, and optical properties of a collection of TM dinuclear molecules using DFT calculations. The geometric structures of molecules are optimized within the gas phase, and their structural stability were analyzed by studying vibrational properties. The right ground-state spin configuration of the tetra-coordinated TM atom in each molecule was estimated by comparing total energies of the molecule in several possible spin-state configurations. We observed that the TM atoms in Cr-

, Mn-, Fe-, Co-, and Ni-dinuclear molecules are in S = 2, S = 5/2, S = 1, S = 1/2 and S = 0 spin state, respectively, within the state. Aside from Mn-dinuclear, the planer structure remains intact altogether other molecules and expected to be adsorbed and self-assembled on metal substrates. Therefore, we anticipate that this class of molecules would be very suitable for molecular spintronic applications. The optical properties of TM dinuclear molecules are calculated using the TD-DFT method. We observe that within the case of Cr-, Mn-, Co-, and Ni-dinuclear molecules, the absorption takes place mainly near blue light wavelength range; therefore, it may be suitable for optoelectronic device applications.

Supporting Information Available

The Supporting Information is offered freed from charge at https://pubs.acs.org/doi/10.1021/acsomega.0c02992.

• Calculated torque on TM atoms within the modelled TM dinuclear molecules with different U values, calculated TM–ligand bond length (in Å) within the geometry of tetra-coordinated TM for the modelled TM dinuclear molecules, calculation of the distortion parameter, and calculated vibrational spectra (PDF)

References

Patai S.; Rappoport Z.. The Chemistry of the Quinonoid Compounds; Wiley: New York, 1988; Vol. 2, Parts 1 and 2.

Lekin K.; Leitch A. A.; Assoud A.; Yong W.; Desmarais J.; Tse J. S.; Desgreniers S.; Secco R. A.; Oakley R. T. Benzoquinone-Bridged Heterocyclic Zwitterions as Building Blocks for Molecular Semiconductors and Metals. Inorg. Chem. 2018, 57, 4757–4770. 10.1021/acs.inorgchem.8b00485.

Elhabiri M.; Siri O.; Sornosa-Tent A.; Albrecht-Gary A.-M.; Braunstein P. Acid–Base Sensors Based on Novel Quinone-Type Dyes. Chem.—Eur. J. 2004, 10, 134–141. 10.1002/chem.200305206.

Su M.; Liu Y.; Ma H.; Ma Q.; Wang Z.; Yang J.; Wang M. 1,9-Dihydro-3-phenyl-4H-pyrazolo[3,4-b]quinolin-4-one, a novel fluorescent probe for extreme pH measurement. Chem. Commun. 2001, 960–961. 10.1039/b101685g.

Izumi Y.; Sawada H.; Sakka N.; Yamamoto N.; Kume T.; Katsuki H.; Shimohama S.; Akaike A. p-quinone mediates 6-hydroxydopamine-induced dopaminergic neuronal death and ferrous iron accelerates the conversion of p-quinone into melanin extracellularly. J. Neurosci. Res. 2005, 79, 849–860. 10.1002/jnr.20382.

Routaboul L.; Braunstein P.; Xiao J.; Zhang Z.; Dowben P. A.; Dalmas G.; Da Costa V.; Félix O.; Decher G.; Rosa L. G.; Doudin B. Altering the Static Dipole on Surfaces through Chemistry: Molecular Films of Zwitterionic Quinonoids. J. Am. Chem. Soc. 2012, 134, 8494–8506. 10.1021/ja212104b.

Kim S. B.; Pike R. D.; Sweigart D. A. Multifunctionality of Organometallic Quinonoid Metal Complexes: Surface Chemistry, Coordination Polymers, and Catalysts. Acc. Chem. Res. 2013, 46, 2485–2497. 10.1021/ar300353n.

Dei A.; Gatteschi D.; Sangregorio C.; Sorace L. Quinonoid metal complexes: Toward molecular switches. Acc. Chem. Res. 2004, 37, 827–835. 10.1021/ar0200706.

Kar P.; Yoshida M.; Shigeta Y.; Usui A.; Kobayashi A.; Minamidate T.; Matsunaga N.; Kato M. Methanol-Triggered Vapochromism Coupled with Solid-State Spin Switching in a Nickel (II)-Quinonoid Complex. Angew. Chem. 2017, 129, 2385–2389. 10.1002/ange.201611085.

Reddy I. R.; Oppeneer P. M.; Tarafder K. Interfacial Spin Manipulation of Nickel-Quinonoid Complex Adsorbed on Co(001) Substrate. Magnetochemistry 2019, 5, 2.10.3390/magnetochemistry5010002.

Kar P.; Yoshida M.; Kobayashi A.; Routaboul L.; Braunstein P.; Kato M. Colour tuning by the stepwise synthesis of mononuclear and homo- and hetero-dinuclear platinum(II) complexes using a zwitterionic quinonoid ligand. Dalton Trans. 2016, 45, 14080–14088. 10.1039/c6dt02328b.

Frisch M. J.; Trucks G. W.; Schlegel H. B.; Scuseria G. E.; Robb M. A.; Cheeseman J. R.; Scalmani G.; Barone V.; Petersson G. A.; Nakatsuji H.; et al.Gaussian 09, 2009; Gaussian Inc: Wallingford CT.

Schäfer A.; Huber C.; Ahlrichs R. Fully optimized contracted Gaussian basis sets of triple zeta valence quality for atoms Li to Kr. J. Chem. Phys. 1994, 100, 5829–5835. 10.1063/1.467146.

Ali M. E.; Sanyal B.; Oppeneer P. M. Electronic structure, spin-states, and spin-crossover reaction of heme-related Fe-porphyrins: a theoretical perspective. J. Phys. Chem. B 2012, 116, 5849–5859. 10.1021/jp3021563.

Tao J.; Perdew J. P.; Staroverov V. N.; Scuseria G. E. Climbing the density functional ladder: Nonempirical meta–generalized gradient approximation designed for molecules and solids. Phys. Rev. Lett. 2003, 91, 146401.10.1103/physrevlett.91.146401.

Staroverov V. N.; Scuseria G. E.; Tao J.; Perdew J. P. Comparative assessment of a new nonempirical density functional: Molecules and hydrogen-bonded complexes. J. Chem. Phys. 2003, 119, 12129–12137. 10.1063/1.1626543.

Jensen K. P.; Cirera J. Accurate Computed Enthalpies of Spin Crossover in Iron and Cobalt Complexes. J. Phys. Chem. A 2009, 113, 10033–10039. 10.1021/jp900654j.

Kresse G.; Furthmüller J. Efficient iterative schemes for ab initio total-energy calculations using a plane-wave basis set. Phys. Rev. B: Condens. Matter Mater. Phys. 1996, 54, 11169–11186. 10.1103/physrevb.54.11169.

Blöchl P. E. Projector augmented-wave method. Phys. Rev. B: Condens. Matter Mater. Phys. 1994, 50, 17953–17979. 10.1103/physrevb.50.17953.

Perdew J. P.; Burke K.; Ernzerhof M. Generalized Gradient Approximation Made Simple. Phys. Rev. Lett. 1996, 77, 3865–3868. 10.1103/physrevlett.77.3865.

Dudarev S. L.; Botton G. A.; Savrasov S. Y.; Humphreys C. J.; Sutton A. P. Electron-energy-loss spectra and the structural stability of nickel oxide: An LSDA+ U study. Phys. Rev. B 1998, 57, 1505.10.1103/physrevb.57.1505.

Tarafder K.; Kanungo S.; Oppeneer P. M.; Saha-Dasgupta T. Pressure and Temperature Control of Spin-Switchable Metal-Organic Coordination Polymers from Ab Initio Calculations. Phys. Rev. Lett. 2012, 109, 077203.10.1103/physrevlett.109.077203.

Wäckerlin C.; Tarafder K.; Siewert D.; Girovsky J.; Hählen T.; Iacovita C.; Kleibert A.; Nolting F.; Jung T. A.; Oppeneer P. M.; Ballav N. On-surface coordination chemistry of planar molecular spin systems: novel magnetochemical effects induced by axial ligands. Chem. Sci. 2012, 3, 3154–3160. 10.1039/c2sc20828h.

Reddy I. R.; Oppeneer P. M.; Tarafder K. Route to achieving giant magnetoelectric coupling in $BaTiO_3/Sr_2CoO_3F$ perovskite heterostructures. Phys. Rev. B 2018, 98, 140401.10.1103/physrevb.98.140401.

Wäckerlin C.; Tarafder K.; Girovsky J.; Nowakowski J.; Hählen T.; Shchyrba A.; Siewert D.; Kleibert A.; Nolting F.; Oppeneer P. M.; Jung T. A.; Ballav N. Ammonia Coordination Introducing a Magnetic Moment in an On-Surface Low-Spin Porphyrin. Angew. Chem., Int. Ed. 2013, 52, 4568–4571. 10.1002/anie.201208028.

Xing X.; Hermann A.; Kuang X.; Ju M.; Lu C.; Jin Y.; Xia X.; Maroulis G. Insights into the geometries, electronic and magnetic properties of neutral and charged palladium clusters. Sci. Rep. 2016, 6, 19656.10.1038/srep19656.

Ju M.; Lv J.; Kuang X.-Y.; Ding L.-P.; Lu C.; Wang J.-J.; Jin Y.-Y.; Maroulis G. Systematic theoretical investigation of geometries, stabilities and magnetic properties of iron oxide clusters $(FeO)_n^{\mu}$(n= 1–8, μ= 0,±1): insights and perspectives. RSC Adv. 2015, 5, 6560–6570. 10.1039/c4ra12259c.

Zhang Y. Electronegativities of elements in valence states and their applications. 1. Electronegativities of elements in valence states. Inorg. Chem. 1982, 21, 3886–3889. 10.1021/ic00141a005.

Li K.; Xue D. Estimation of Electronegativity Values of Elements in Different Valence States. J. Phys. Chem. A 2006, 110, 11332–11337. 10.1021/jp062886k.

Hauser A.Spin Crossover in Transition Metal Compounds I; Springer, 2004; pp 49–58.

Adamo C.; Barone V. Toward reliable density functional methods without adjustable parameters: The PBE0 model. J. Chem. Phys. 1999, 110, 6158–6170. 10.1063/1.478522.

Hay P. J.; Wadt W. R. Ab initio effective core potentials for molecular calculations. Potentials for the transition metal atoms Sc to Hg. J. Chem. Phys. 1985, 82, 270–283. 10.1063/1.448799.

Chiodo S.; Russo N.; Sicilia E. LANL2DZ basis sets recontracted in the framework of density functional theory. J. Chem. Phys. 2006, 125, 104107.10.1063/1.2345197.